Desalination with Electrodialysis as Energy Buffer in Polygeneration Systems: dynamic simulations and control strategy

Antonino Campione[1], Andrea Cipollina[1]*, Francesco Calise[2], Alessandro Tamburini[1], Mosè Galluzzo[1], Giorgio Micale[1]

1 Dipartimento di Ingegneria (DI), Università degli Studi di Palermo, viale delle scienze ed. 6, 90128 Palermo –Italy

2 Department of Industrial Engineering, University of Naples Federico II, Naples, Italy- Piazzale Tecchio 80, 80125 Napoli, Italy

*andrea.cipollina@unipa.it

The presence of desalination systems in polygeneration facilities is usually limited by important difficulties in operating under non-stationary regimes. The possibility of using electrodialysis coupled with a hybrid photovoltaic/wind energy source was investigated in this work. In particular, the combination of photovoltaic and wind energy is very attractive in order to achieve a more stable energy production. Dynamic scenarios were analysed, looking at two different time scales. Quasi steady-state simulations were used to study the yearly operation, demonstrating process flexibility over a power input variation of one order of magnitude (5-45 kW). Dynamic simulations were adopted to study the daily time scale, where the desalination unit control system, purposely designed and tuned, was able to maintain a stable target value (± 10%) in presence of disturbances in power availability. Simulation results show how the ED process is particularly suitable for the integration within polygeneration systems as energy-buffer.

KEYWORDS

Solar energy; time dependent; Renewable energy; cogeneration; desalination; process control

1. INTRODUCTION

Desalination units can generally be part of polygeneration facilities. Waste heat from thermal power plants has been used to successfully run thermal desalination plants [1] or to preheat salt water feeds [2]. In this context, polygeneration systems that use renewable sources such as photovoltaic (PV) or wind turbines represent a promising scenario [3]. In these cases, desalination technologies can be particularly attractive as means of using the excess energy that renewable sources produce during peak periods, producing drinking water instead of using energy storage devices such as batteries [4].

One of the main issues related to the use of renewable polygeneration systems consists in the unpredictability of the energy source. The unavoidable fluctuations of many renewable energy sources (wind, solar, etc.) make extremely difficult to suitably couple these systems with the cooling, heating and electrical demands of the users [5]. In this framework, many researchers investigated several storage technologies (both thermal and electrical) in order to achieve a more stable power supply profile [6]. However, such storage technologies are still too expensive for a good economic profitability. Therefore, some researchers are focusing on innovative solutions such as coupling renewables and desalination systems [7–13]. Simultaneously, many authors are focusing on specific combinations of renewable energy sources in order to mitigate

the fluctuations typical of using individual renewable energy sources. For example, the combination of solar and wind energy is extremely promising. In fact, solar energy is mainly available during the summer and in the central hours of the day. Conversely, according to the weather data, wind velocity increases in winter and during the night. Therefore, combining photovoltaic solar energy and wind energy the stability of power production profile can be increased.

The possibility to couple desalination systems with renewable energy sources has been already demonstrated in the literature. Given the wider commercial diffusion of reverse osmosis (RO) among desalination technologies, a lot of works focus on this process. In particular, process feasibility has been studied and proven for PV-RO [14–22], wind-RO [23,24] and combined PV and wind-RO systems [25]. A number of these works highlight how the economic feasibility of such processes can be enhanced using battery-less power sources, as batteries are associated to a number of disadvantages such as increased capital costs, limited lifetime and increased maintenance [17,24]. Nevertheless, when desalination units are coupled with battery-less systems they are directly subjected to the fluctuation of power generation, requiring real-time adjusting. Thomson et al. [21,22] demonstrated the possibility to apply such systems to RO from both modelling and experimental perspective. However, the authors (as well as Manolakos et al. in another work [14]) highlighted that long term reliability of the system is not guaranteed due to the continuous high pressure fluctuation experienced by membranes. An alternative to compensate for the power fluctuation, by modifying the production capacity without significantly affect the pressure, is the use a number of parallel RO plants that are switched on or off based on the amount of energy available [23]. Nevertheless, this generally implies a system oversizing and an increase in capital costs. Besides the aforementioned issues, RO systems also suffer from relatively slow and critical start-ups and shutdowns where a gradual increase/decrease in system pressure is required before reaching the steady-state [23].

On the other hand, experimental investigation on ED systems working with renewable energy sources is ongoing since few decades ago [26,27]. In general, ED can overcome most of the drawbacks that result from dynamic RO operations. A change in the available power input can be easily adjusted by changing the applied voltage and by changing the feed flowrate without the need for particular adjustments, as low pressures (usually < 1 barg) are involved in the process. Another advantage is that transient phases during start-ups and shutdowns are much shorter. Conversely, the main issue that has been highlighted refers to an increased energy consumption due to the presence of harmonic disturbances that can be mitigated through filters [23]. For these reasons, ED is particularly suitable for battery-less systems. In this context, Malek et al. [28] showed a successful experimental coupling of batch ED with direct wind energy, demonstrating how the system is insignificantly affected by moderate wind fluctuations. Similarly, Ortiz et al. [29–31] proved the operation of a batch PV-ED system through experiments and simulations in the scale of hours. In addition, from cost estimations, PV-ED resulted more convenient than PV-RO in the presence of low salinity feeds [15].

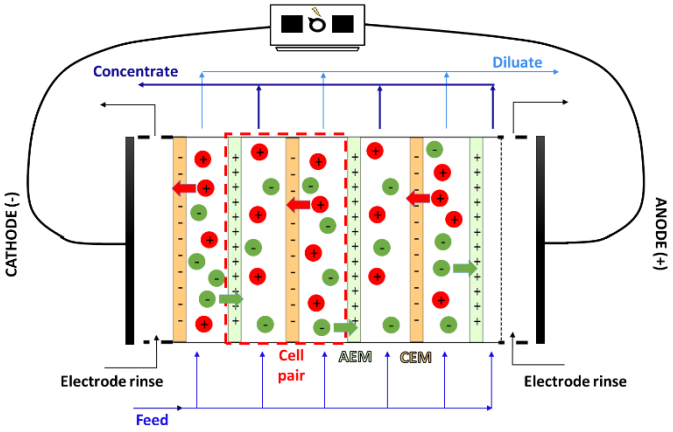

Figure 1. Scheme of the ED process. Adapted from [32].

As already highlighted, most of the works on ED coupled with renewable sources focus on the experimental proof of concept, on coupled process design or on economic analysis. In fact, attention to the detailed process dynamics is mostly paid only in the case of batch ED, where the effect of power fluctuations on the product quality are strongly dampened by the presence of recirculation tanks. Therefore, the aim of the present work was to study the dynamics of a single pass ED unit powered by a hybrid PV/wind power source in order to prove the flexibility of ED in maintaining drinking water specifications while changing process conditions, assessing the suitability for integration within poly-generation systems as energy-buffer. In particular, the analysis was performed by means of process simulations, focusing on two different time-scales. The first one is the yearly operational time scale, where quasi-stationary operation of ED allows for a step by step re-adaptation of working parameters in order to generate a stable output target with the available energy input. The other one is the short time scale of transient regimes of the desalination unit, where the intrinsically dynamic behaviour of the unit was modelled to predict the response to fast disturbances in energy availability. At this scale, a control system was also designed and implemented.

2. MODELLING

The overall simulation model was implemented by a hybrid approach combining a well-known dynamic simulation tool, TRNSYS [33] , and a user-developed model. In particular, the model for the solar/wind system is developed in TRNSYS by using weather data from Pantelleria, and conventional components included in TRNSYS library (PV panels, wind turbine, inverter, controllers, etc). The overall electrical production calculated by TRNSYS is subsequently provided as an input data to the user-developed model, simulating the ED subsystem implemented into *gPROMS Modelbuilder*. In the followings, the main algorithms of the models are briefly presented

2.1 PV panels

In order to simulate the PV panels, the four parameter model was used. It assumes that the slope of the IV curve is zero at the short-circuit condition:

$$\left(\frac{dI}{dV}\right)_{v=0} = 0 \qquad (1)$$

The four parameters included in the model are: i) $I_{L,ref}$ (module photocurrent at reference

conditions), ii) $I_{o,ref}$ (diode reverse saturation current at reference conditions), iii) γ (empirical PV curve-fitting parameter), iv) R_s (module series resistance). The software uses parameters values from manufacturers' data in order to generate an IV curve at each time step.

The current-voltage equation of the circuit is:

$$I = I_{L,ref}\frac{G_T}{G_{T,ref}} - I_o\left[\exp\left(\frac{q}{\gamma k T_c}\left(V + IR_s\right)\right) - 1\right] \quad (2)$$

where G_T and $G_{T,ref}$ are the insolation and the reference insolation respectively, q is the electron charge, k is the Boltzmann constant and T_c is the temperature of the cells.
The diode reverse saturation current I_o is a temperature dependent function, such as:

$$\frac{I_o}{I_{o,ref}} = \left(\frac{T_c}{T_{c,ref}}\right)^3 \quad (3)$$

where $I_{o,ref}$ is one of the four parameters defined above.
Once I_o is obtained, the Newton's method is employed to calculate the PV current, whereas an iterative search routine finds the current (I_{mp}) and voltage (V_{mp}) at the point of maximum power along the IV curve. To solve the four equivalent circuit characteristics, current and voltage at open-circuit, short circuit, and maximum power conditions are substituted into eq. (2), yielding, after some rearrangement, to the following three eqs. (4)-(6) related to $I_{L,ref}$, $I_{o,ref}$, γ:

$$I_{L,ref} \approx I_{sc,ref} \quad (4)$$

$$\gamma = \frac{q\left(V_{mp,ref} - V_{oc,ref} + I_{mp,ref}R_s\right)}{kT_{c,ref}\ln\left(1 - \frac{I_{mp,ref}}{I_{sc,ref}}\right)} \quad (5)$$

$$I_{o,ref} = \frac{I_{sc,ref}}{\exp\left(\frac{qV_{oc,ref}}{\gamma k T_{c,ref}}\right)} \quad (6)$$

A fourth equation, eq. (7), derived by taking the analytical derivative of voltage with respect to temperature at the reference open-circuit condition, is needed in order to determine the last unknown parameter:

$$\frac{\partial V_{oc}}{\partial T_c} = \mu_{voc} = \frac{\gamma k}{q}\left[\ln\left(\frac{I_{sc,ref}}{I_{o,ref}}\right) + \frac{T_c\mu_{isc}}{I_{sc,ref}} - \left(3 + \frac{q\varepsilon_G}{\frac{\gamma}{N_M}kT_{c,ref}}\right)\right] \quad (7)$$

This analytical value is matched to the open circuit temperature coefficient (manufactures' specification). Finally, an iterative search routine is followed to calculate the equivalent circuit characteristics.

2.2 Wind Turbine

The model calculates the power output P of the WT through the power coefficient of WT, c_p, multiplied by the area of the rotor and the wind power, as reported in eq. (8):

$$P = \rho c_p A_r v^3 = \rho 4a\left(1-a\right)^2 A_r v^3 \quad (8)$$

here, v is the wind speed (m/s), A_r is the rotor area (m^2) and ρ is the air density (kg/m^3). The c_p is a function of the axial induction factor, a, and its maximum value of 59.3%, obtained for a = 1/3, was first derived by Betz in 1919 (known as Betz's limit).
The WT power calculation is based on a power versus wind speed characteristic (Figure 2), provided by the manufacturer.

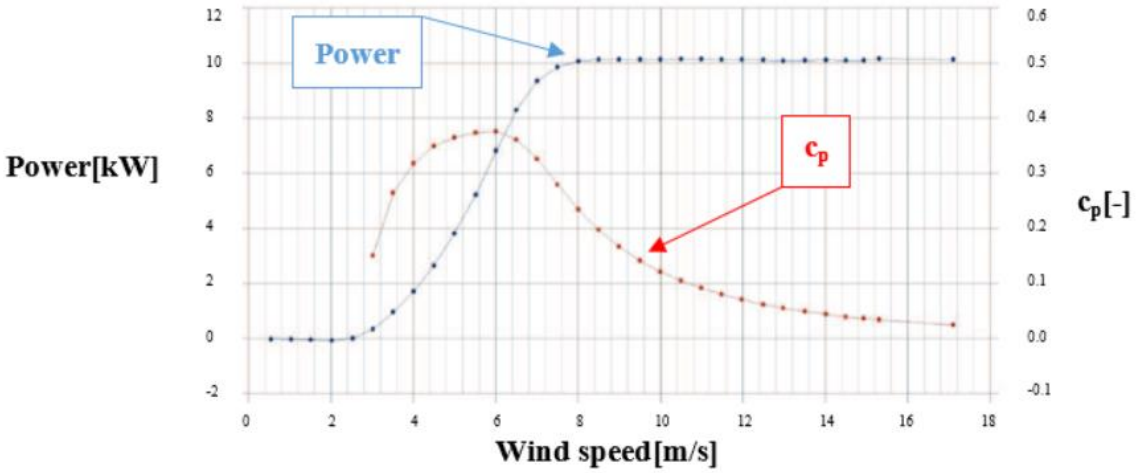

Figure 2. Power (left) and c_p (right) versus wind speed characteristic curve.

This model takes into account the air density changes and wind speed increases with height above the ground (elevation). Air density at a certain elevation is a function of the combined effects of pressure and temperature, according to the ideal gas law, and it is calculated as:

$$\rho_{elev} = \frac{p_{elev}}{RT} \quad (9)$$

Regarding the variability of the temperature as a function of the elevation, the temperature "lapse rate" is also considered as shown in eq.(10):

$$T(z) = T_0 - B\,z \quad (10)$$

where B = 6.5 K/km of altitude and T_0= 288K.

The change in wind speed per change in height above the ground is based on the theoretical work of Von Karman [34]. Here, the relation between the elevation and the wind speed is formulated as follows:

$$\frac{v_1}{v_2} = \left(\frac{z_1}{z_2}\right)^{\alpha_w} \quad (11)$$

A single parameter, α_w, determines the rate of wind speed increase as a function of height. Under ideal boundary layer conditions, the value of α_w is 1/7 (0.14). However, under actual conditions, the value of α_w constantly varies, and depends on a plurality of factors, affecting vertical turbulence intensity (surface roughness, mountains, buildings, atmospheric stability, etc.).

Table 1. Main design parameters of wind turbine and PV panels.

	Parameter	Description	Value	Unit
PV PANELS	$A_{module,PV}$	PV module area	1.609	m^2
	$P_{module,PV}$	Unit peak power	260	W
	$I_{sc,ref}$	Module short-circuit current at reference conditions	6.50	A
	$V_{oc,\ ref}$	Module open-circuit voltage at reference conditions	21.6	V
	$T_{c,\ ref}$	Reference temperature	298	K
	$G_{T,ref}$	Reference insolation	1000	W/m^2
	$V_{mp,ref}$	Module voltage at max power point and reference conditions	17	V
	$I_{mp,ref}$	Module current at max power point and reference conditions	5.9	A
	μ_{Isc}	Temperature coefficient of I_{sc} at (ref. condition)	0.02	A/K
	μ_{voc}	Temperature coefficient of V_{oc} (ref. condition)	-0.079	V/K
	$T_{c,\ NOCT}$	Module temperature at NOCT	313	K
	$T_{c,\ ref}$	Ambient temperature at NOCT	293	K
WIND TURBINE	z	Site elevation	205	m
	H	Data collection Height	18	m
	H_{hub}	Hub height	10.2	m
	N_{WT}	Number of turbines	1	-
	P_{WT}	Wind turbine rated power	10	kW
	v_{rated}	Wind turbine rated speed	6.5	m/s
	$v_{cut,in}$	Cut-in speed	2.6	m/s
	$v_{cut,off}$	Cut-off speed	16	m/s

2.3 Electrodialysis process

The studies presented in this work are based on a steady-state hierarchical ED model (scheme is reported in Figure 3) [32] that has been modified to account for the dynamic behaviour of the system.

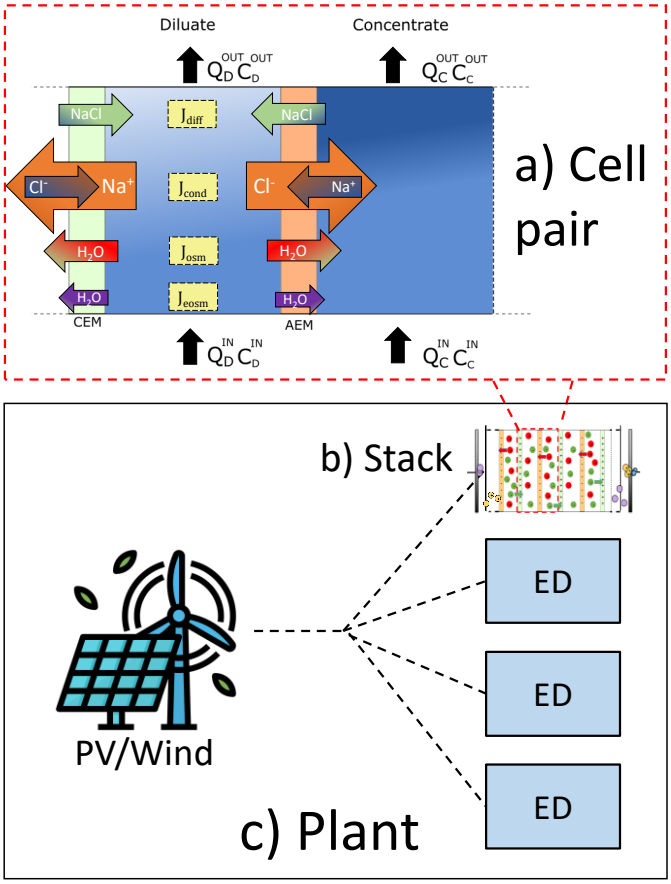

Figure 3. Scheme of the hierarchies of the ED process model representing: a) the cell pair model, b) the stack model and c) the overall plant model.

The lowest hierarchy of the model (Figure 3 a), i.e. the cell pair, is the repeating unit of the system, including an anion-exchange membrane (AEM), a diluate channel, a cation-exchange membrane (CEM) and a concentrate channel. At this scale, material balances and transport phenomena are described. In particular, the dynamic, 1D mass balances in a generic (concentrate or diluate) channel can be written as:

$$b\delta_{SOL}\frac{\partial C_{SOL}(x,t)}{\partial t}+\frac{\partial Q_{SOL}(x,t)C_{SOL}(x,t)}{\partial x}=\pm b\,J_{tot}(x,t) \tag{12}$$

$$\frac{d\,Q_{SOL}(x,t)}{dx}=\pm\,b\,q_w(x,t) \tag{13}$$

where A is the membrane active area, δ_{SOL} is the channel thickess, C_{SOL} is the salt concentration in solution, b is the channel width, J_{tot} is the total salt flux through the membranes (i.e. the sum of conductive and diffusive salt flux [32]), Q_{SOL} represents the local volumetric flow rate of a single cell pair, and q_w the local overall volumetric water flux through the membranes (i.e. the sum of osmotic and electroosmotic fluxes [32]). t and x indicates that the variables are function of time and space (i.e. the axial direction of the solution flow through the channels).

Electrical variables of the cell pair are also computed. In particular, the cell pair voltage drop (V_{cp}) can be written as:

$$V_{cp}(t) = \eta(x,t) + R_{tot}(x,t)\, i(x,t) \tag{14}$$

where η is the non-Ohmic voltage drop associated to the back electromotive force where concentration polarisation is also taken into account making use of computationally determined Sherwood numbers [32,35–37], i is the local current density and R_{tot} is the total areal Ohmic resistance of cell pair which can be calculated as the sum of membrane and solution compartment resistances [32].

A number of cell pairs are grouped together in the Stack higher hierarchy (Figure 3 b), where the external applied voltage (V_{tot}) is related to the internal electric variables:

$$V_{tot}(t) = \frac{R_{blank} I}{A} + \sum_{i=1}^{N_{cp}} V_{cpi}(t) \tag{15}$$

where, R_{blank} is the blank resistance, accounting for electric voltage drops in the electrode compartments, I is the total current, calculated as the integral of the current density over the active area, and N_{cp} is the number of cell pairs inside the stack.

The stack model also computes performance parameters such as current efficiency and specific energy consumption [32].

Finally, the stack can be implemented in the highest hierarchy of the plant (Figure 3 c). In the case of this work, the stack model was coupled with a variable power source and a control unit (Figure 4). The details of the controller equation, as well as its design and tuning are discussed in the control design section.

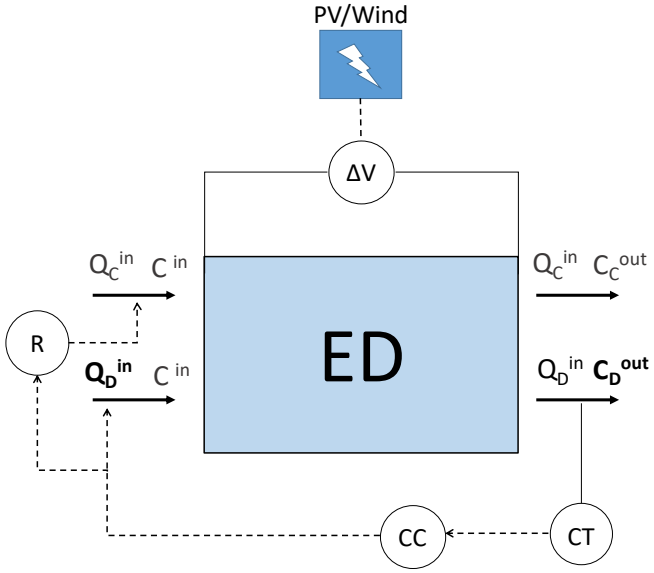

Figure 4. Detailed block diagram of the highest hierarchy of the model (the plant) representing an ED unit powered by the PV/wind power delivery system. The control system of the product concentration, acting on the feed flowrate is also shown.

3. LONG TIME SCALE SIMULATIONS

The aim of this work was to simulate an ED unit powered by a variable hybrid PV/Wind energy source. In particular, the energy system includes a 20 kW wind turbine and a PV array with a peak of power production of about 25 kW, for a total peak power production of about 45 kW. The energy supply system was simulated over an entire year.

The ED plant is composed by 4 equal stacks operating in parallel that have to desalinate a feed stream of 5g/l NaCl concentration down to 0.25 g/l with 67% recovery (i.e. the diluate to concentrate feed flowrate ratio is always kept constant to 2:1, as indicated in Figure 4) . Stacks' specifications are listed in Table 2.

Table 2.List of the main characteristics of each simulated ED stack.

L (cm)	b (cm)	N_{cp}	δ_{SOL} (μm)	Type of membranes	R_{blank} (Ωcm^2)
50	50	500	270	FUJIFILM Type 10	3

At nominal conditions, the plant works with ~80% of the peak power (34 kW), producing 800 m^3/d (200 per stack) of drinking water. However, the actual diluate flowrate changes according to the available power, in order to keep a constant outlet concentration. Based on feasibility conditions, upper and lower limits were set in each stack for the diluate flowrate. In particular, the maximum diluate feed flowrate was set according to the maximum allowable pressure drop that has been set to 1.2 bar, corresponding to 920 m^3/d (230 m^3/d per stack) and 43 kW of absorbed power. Conversely, the minimum allowable flowrate was set to ~ 230 m^3/d (58 m^3/d per stack) and 5 kW of absorbed power, where the current required to reach 0.25 g/l is already 90% of the estimated limiting current [38]. Further reduction in the diluate feed flowrate would cause limiting current issues and thus an impossibility to reach the target concentration.

According to the aforementioned limits, the ED system was simulated assuming that the applied voltage was changing depending on the power produced by the energy system over the entire year. The boundaries were taken into account, so that if the available power is higher than the upper limit the plant does not use all of it. Conversely, when the power is lower than the minimum the system is switched off. Given the long time scale, a quasi-steady state approach was adopted for these simulations.

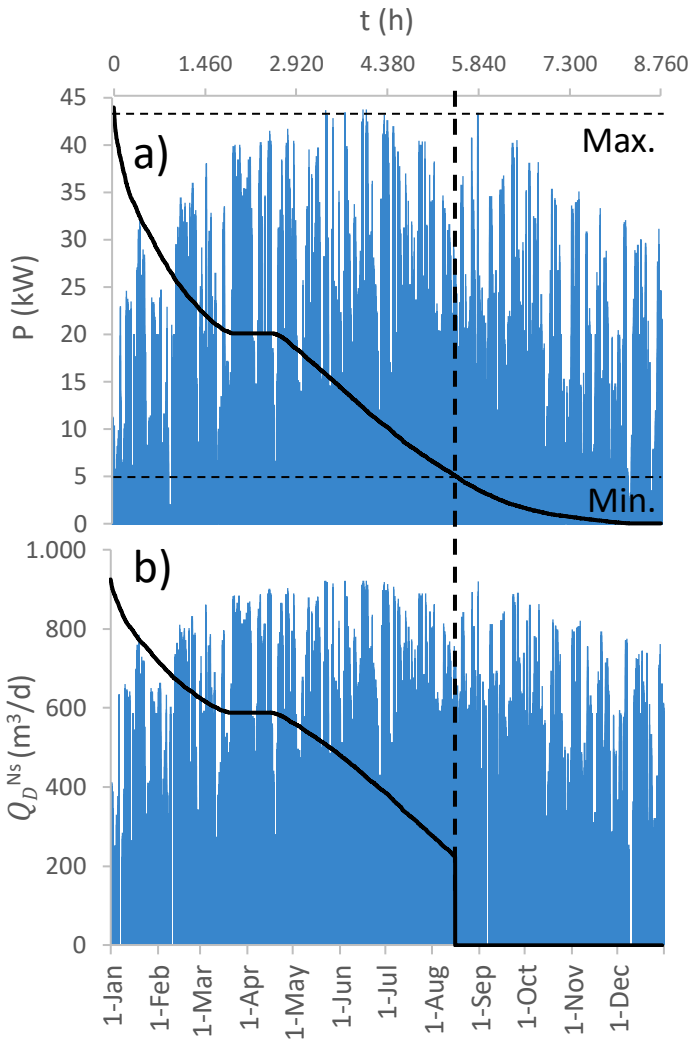

Figure 5. a) Simulated yearly power production for the coupled PV/Wind energy source, b) Simulated feed flowrate in the 4 ED units operating in parallel. Vertical bars represent the hourly variation, while the black lines are the cumulative curves for the two variables. ED units specifications: 50x50 cm^2, 500 cell pairs, 270 μm spacers and FUJIFILM Type 10 membranes.

Figure 5 a, shows how much the overall power can be different during the year (according to weather data from Pantelleria). In particular, peaks are clearly more frequent in summer months, when the PV system has more solar radiation available. Produced power goes slightly down in the other periods of the year, even though the wind turbine partially compensates the reduction of solar radiation.

Figure 5 b, shows the diluate feed flowrate of the ED plant (Q_D^{Ns}). As expected, the plant can adapt the feed flowrate to the produced power, and thus generating different amounts of drinking water. Interestingly, the set maximum and minimum flowrate boundaries do not excessively influence the power utilisation on the yearly time scale. In fact, the plant never goes off for long periods except for few phases during winter months, while only very few power peaks are not entirely used during the summer. Figure 4 also shows cumulative curves (black continuous lines) that gives an estimation of the total amount of hours in which power or flowrate were maintained above a certain value. From these curves it can be seen how the plant stays on for more than 5500 (non-continuous) hours during the entire year. In addition, it is

interesting to note that the specific energy consumption decreases while reducing the feed flowrate. This is to be attributed to the operating conditions that are closer to reversibility when the applied voltage is small.

4. CONTROL SYSTEM DESIGN AND TUNING

As the ED unit is powered by a variable power source (i.e. the coupled PV/Wind plant) the actual energy that is available for the desalination process and, thus, the external applied voltage will change over time. The desalination unit has to maintain the outlet concentration of the drinking water at the target value. Therefore, a control system is required in order to adapt continuously the feed flowrate to ensure that the outlet specifications are met. For this reason, the system dynamics was first studied with the aim of defining transfer functions, which link the inlet variables (i.e. feed flow rate and applied voltage) to the outlet variables (i.e. the product concentration) and can be assumed as simplified mathematical descriptions of the nonlinear process. The results of this analysis was then used to define the control strategies and tune the controller. For the sake of simplicity, the control loop takes into account only process dynamics, neglecting other contributions such as the regulation valve.

4.1 Uncontrolled process dynamics

In order to study the process dynamics, it is necessary to characterise the behaviour of the process under transient regime when the manipulation variable (i.e. the flowrate) shifts from the stationary value. Given the nature of the process under study, it is not possible to define a unique reference stationary value, as this will depend on the available power. Therefore, three reference scenarios were chosen, so that it was also possible to assess how the dynamics changes with the starting condition. In particular, the maximum and the minimum allowable flowrates (as discussed in the long time scale simulation section) as well as the average flowrate have been taken as a reference. In each scenario, the flowrate has been either increased or decreased by 20% through a step change.

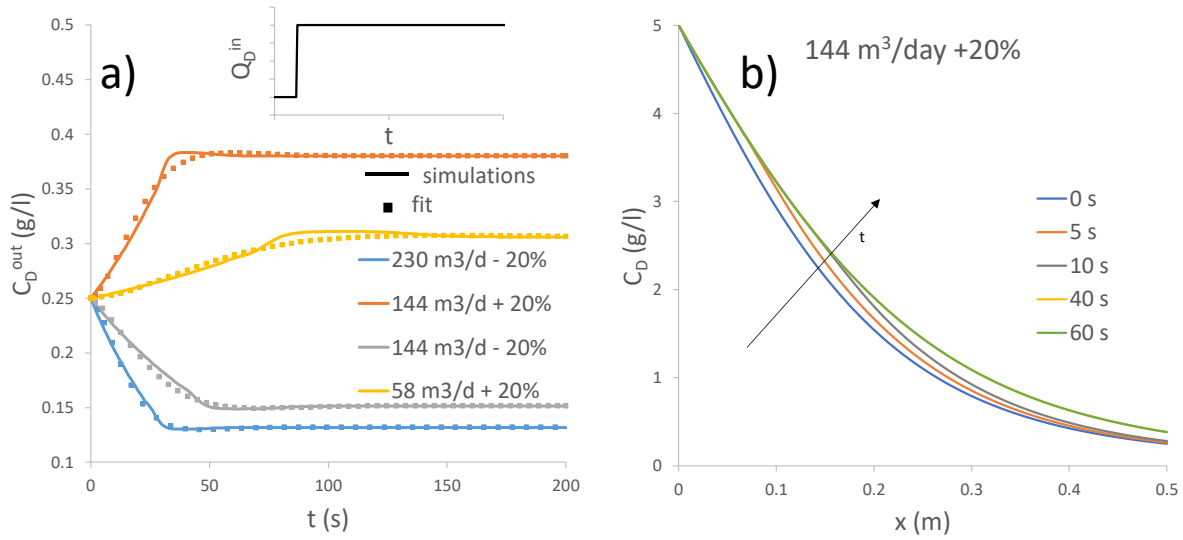

Figure 6. a) Outlet diluate concentration vs. time for a 20% step change in the feed flowrate at different initial diluate flowrates, b) Spatial profile of the outlet diluate concentration at different times for a 20% flowrate step increase starting from 144 m^3/d. Results refer to a 50x50 cm^2 ED unit equipped with 500 cell pairs, 270 µm spacers and FUJIFILM Type 10 membranes.

Figure 6 a shows time profiles of the diluate outlet concentration after the step change. At each steady state flowrate, the voltage is set in order to reach 0.25 g/l. Therefore, when the flowrate increases or decreases, the concentration will reach a new steady state with a higher or lower concentration respectively, requiring a certain time that depends on the flowrate itself. When the flowrate is suddenly changed, the spatial concentration profile in each channel will have to adapt to the new situation (see Figure 6 b), requiring a mutual interaction between each adjacent discretisation interval, through which a certain volume of solution is flowing. Therefore, the resulting dynamic is given by a number of "virtual" processes that occur in sequence and results in a high-order behaviour. However, for the sake of simplicity, each of the curves of Figure 6 a was fitted with a second-order transfer function with a zero that, in the Laplace domain is expressed as:

$$G(s) = \frac{K\,\tau_0 s + K}{s + 2\zeta\tau s + 1} \tag{16}$$

where K is the process gain, τ_0 is the time constant of the transfer function numerator, τ is the process time constant, ζ is the damping coefficient and s is the independent variable in the Laplace domain. Each fitting curve from Figure 6, a was characterised by its own parameters according to eq. (16).

4.2 Feedback control design

The aim of the Feed-Back (FB) control is to keep the target concentration by adjusting the feed flowrate, according to the following equation:

$$Q_D^{in,tot}(t) = K_C\left(\varepsilon + \frac{1}{\tau_I}\int_0^t \varepsilon\,dt + \tau_D\frac{d\varepsilon}{dt}\right) + Q_{D,\,ss}^{in,tot}(t) \tag{17}$$

where K_C is the control gain, ε is the error (i.e. the difference between the concentration set point and the actual concentration), $Q_D^{in,tot}$ and $Q_{D,ss}^{in,tot}$ are the actual and the steady state diluate

flowrate entering inside a stack and τ_I and τ_D are the integral and derivative time constants of the controller. The controller equation written in this form includes proportional, integral and derivative actions.

In order to design an effective and robust controller for the process under study, it is required to identify the best set of parameters (i.e. K_C, τ_I and τ_D). Among the different design methods, the internal model control (IMC) was used to estimate controller parameters [39]. With the IMC method, it was possible to estimate a first set of control parameters for each reference scenario from the fitted process transfer functions previously identified (Figure 6 a). These parameters were then averaged and finely tuned with a trial and error procedure by simulating the response of the controlled system to step voltage changes on *gPROMS Modelbuilder*. The final values are reported in Table 3.

Table 3. Final values of control parameters.

K_C (m^3 l/ g s)	τ_I (s)	τ_D (s)
0.01	30	15

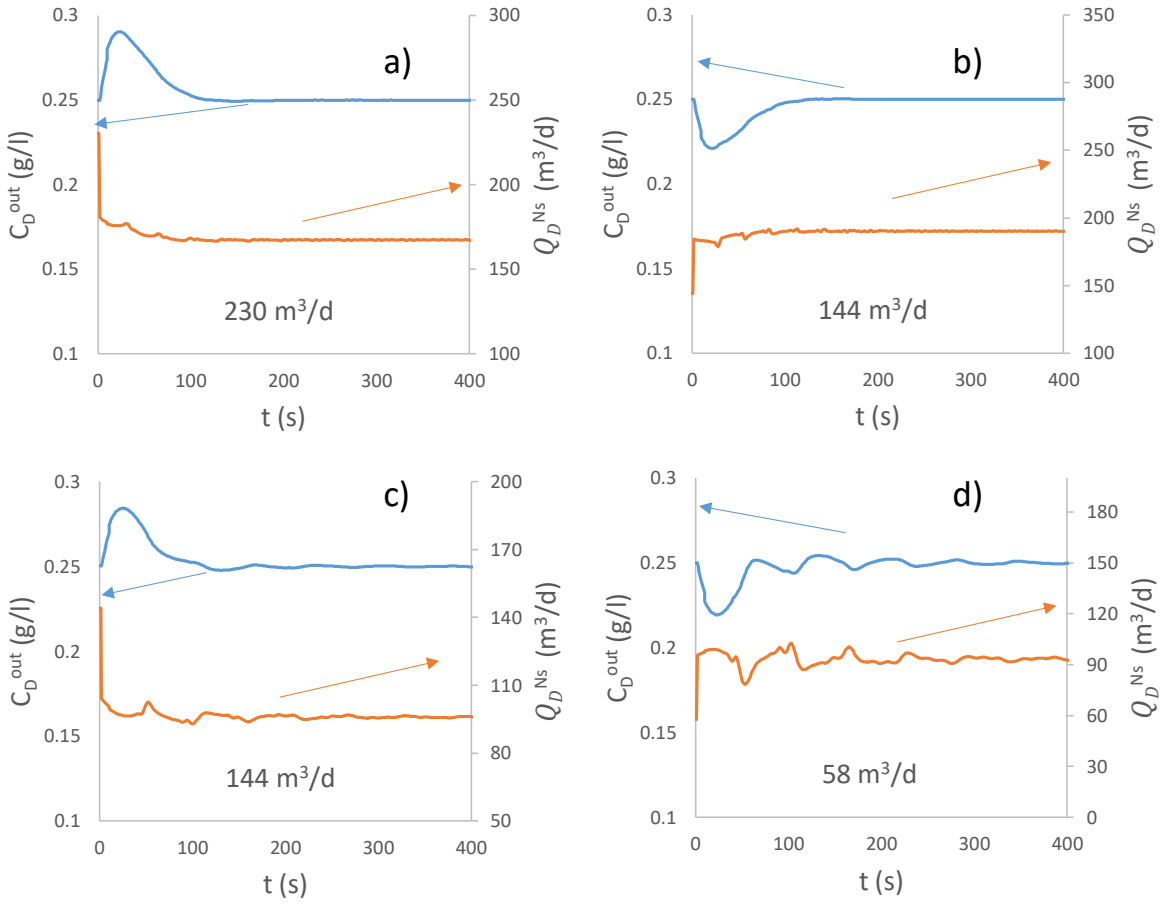

Figure 7. Dynamic ED response of the controlled and the manipulated variables (PID feedback controller) for a voltage step change at different initial diluate feed flowrates. a) 230 m^3/d, 20% voltage decrease, b) 144 m^3/d, 20% voltage increase, c) 144 m^3/d, 20% voltage decrease, d) 58 m^3/d, 20% voltage increase. ED unit specifications: 50x50 cm^2, 500 cell pairs, 270 µm spacers and FUJIFILM Type 10 membranes.

Figure 7 shows simulation results for the controlled ED stack for each reference flowrate. At the maximum flowrate, the system is subjected to a 20% step decrease of the applied voltage (Figure 7 a), the opposite happens for the minimum flowrate (Figure 7 d), while at 144 m3/d both an increase and a decrease of the applied voltage were analysed (Figure 7 b and c). As it can be observed, going from the highest to the lowest flowrate (and thus decreasing the channel velocity), the oscillations of the outlet concentration around the stationary value become more persistent and take more time to settle, even though they are still at an acceptable value. This can be explained by the transient behaviour of the system that changes significantly from high to low flowrates, according to the dynamic responses already shown in Figure 6 a. Besides, a slower response is expected at lower residence times as the process itself needs more time to adapt to the disturbance. It is worth noting that the derivative term was included in the controller in order to dampen the oscillations of the outlet concentration generated by the proportional-integral action of the controller. In particular, excessive decrease in the concentration may cause limiting current issues.

4.3 Feed Forward control design

Given the measurable nature of the main disturbance to the process, namely the available power/voltage at the ED unit, also a Feed Forward (FF) and a hybrid FB-FF controller were designed and tested via simulations. In order to adapt the controller to the strong non-linear behaviour of the process, average gain and time constants were adopted for the design of the controller, leading to a unified law for the FF controller.
The same scenarios adopted for the analysis of the FB controller performance were chosen in this case and results are reported in Figure 8 for the stand-alone FF controller and in Figure 9 for the hybrid FB-FF one.

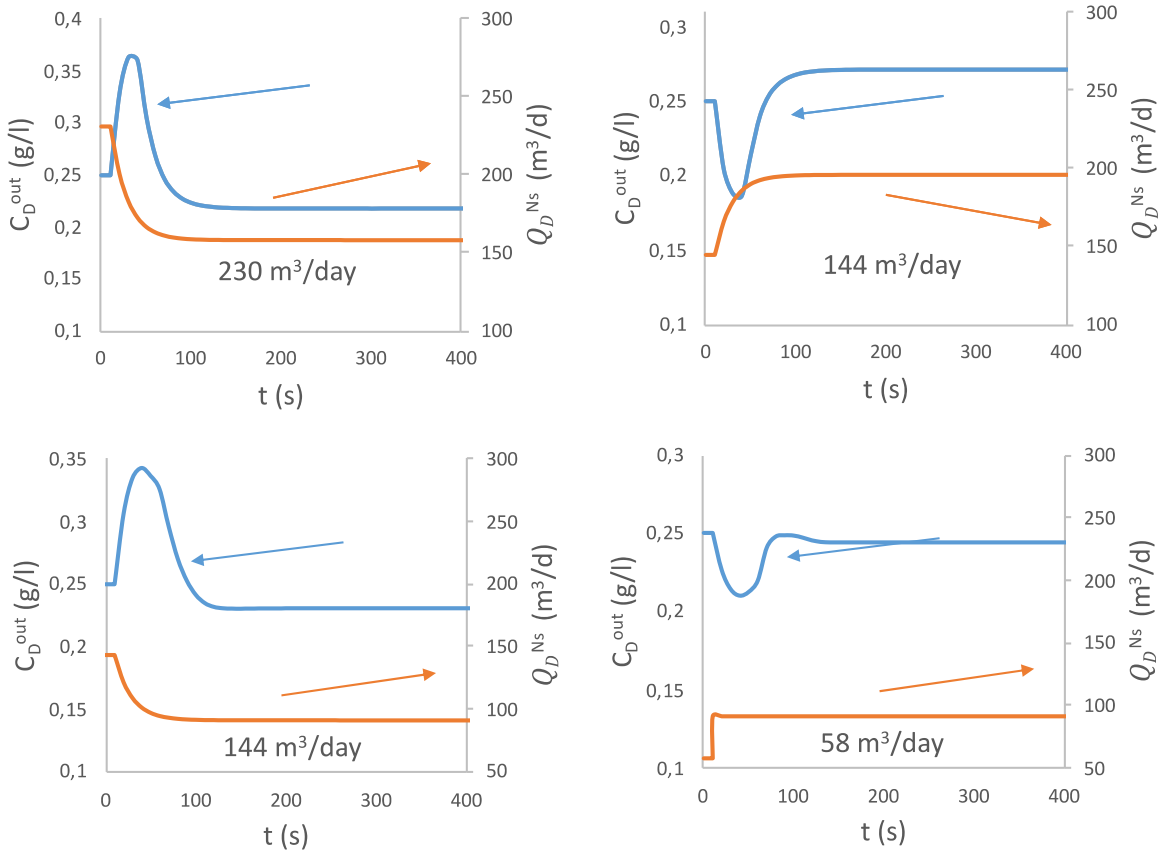

Figure 8. Dynamic ED response of the controlled and the manipulated variables in the case of a stand-alone Feed Forward controller for a voltage step change at different initial diluate feed flowrates. a) 230 m^3/d, 20% voltage decrease, b) 144 m^3/d, 20% voltage increase, c) 144 m^3/d, 20% voltage decrease, d) 58 m^3/d, 20% voltage increase. ED unit specifications: 50x50 cm^2, 500 cell pairs, 270 μm spacers and FUJIFILM Type 10 membranes

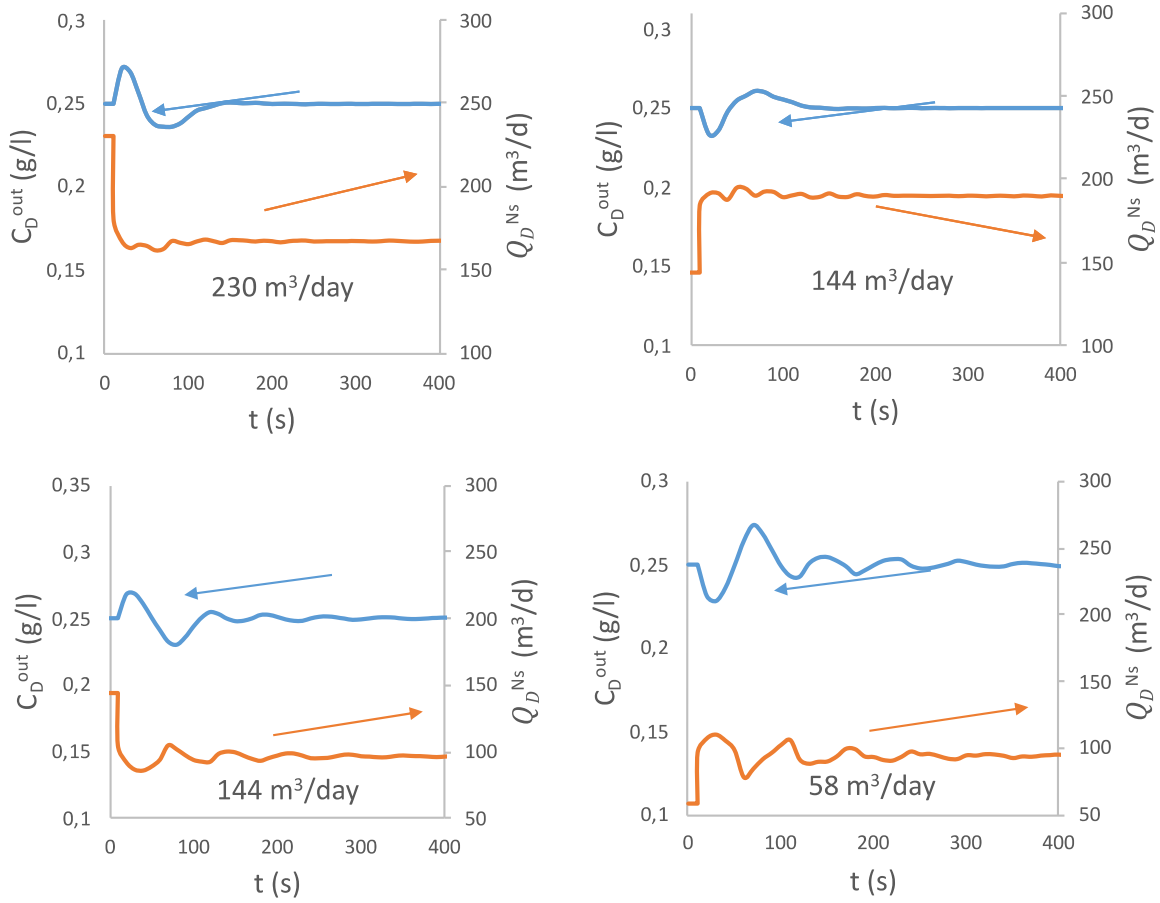

Figure 9. Dynamic ED response of the controlled and the manipulated variables in the case of a hybrid FB-FF controller for a voltage step change at different initial diluate feed flowrates. a) 230 m^3/d, 20% voltage decrease, b) 144 m^3/d, 20% voltage increase, c) 144 m^3/d, 20% voltage decrease, d) 58 m^3/d, 20% voltage increase. ED unit specifications: 50x50 cm^2, 500 cell pairs, 270 μm spacers and FUJIFILM Type 10 membranes.

The implementation of the stand-alone FF controller helps in minimizing the off-set restoring a concentration value close to the target. However, the control is not ideal and some transient deviation from the steady-state value of product concentration is observed.
Looking at the mostly common case of hybrid controller, the response of the system shows several small improvements compared to the simple case of FB controller, both in terms of system stability and amplitude of oscillations.

However, such improvements may have a limited interest in the real cases analysed hereafter due to the smaller and slower disturbances occurring in real operation of solar/wind-powered ED systems. Therefore, the simple FB controller has been adopted for the simulations of short-time-scale scenarios presented in Section 5.

5. SHORT TIME SCALE SIMULATIONS

The dynamic ED model was used to simulate the operation of the controlled ED plant in 4 typical days (from 00:00 to 23:59), that were chosen as representative of the four seasons. At this scale, it is possible to observe the dynamic effect of the control system. For this reason, the voltage applied to the ED units was changed with a 3 minutes step, in order to observe discrete power changes that significantly challenge the stability of the control system.

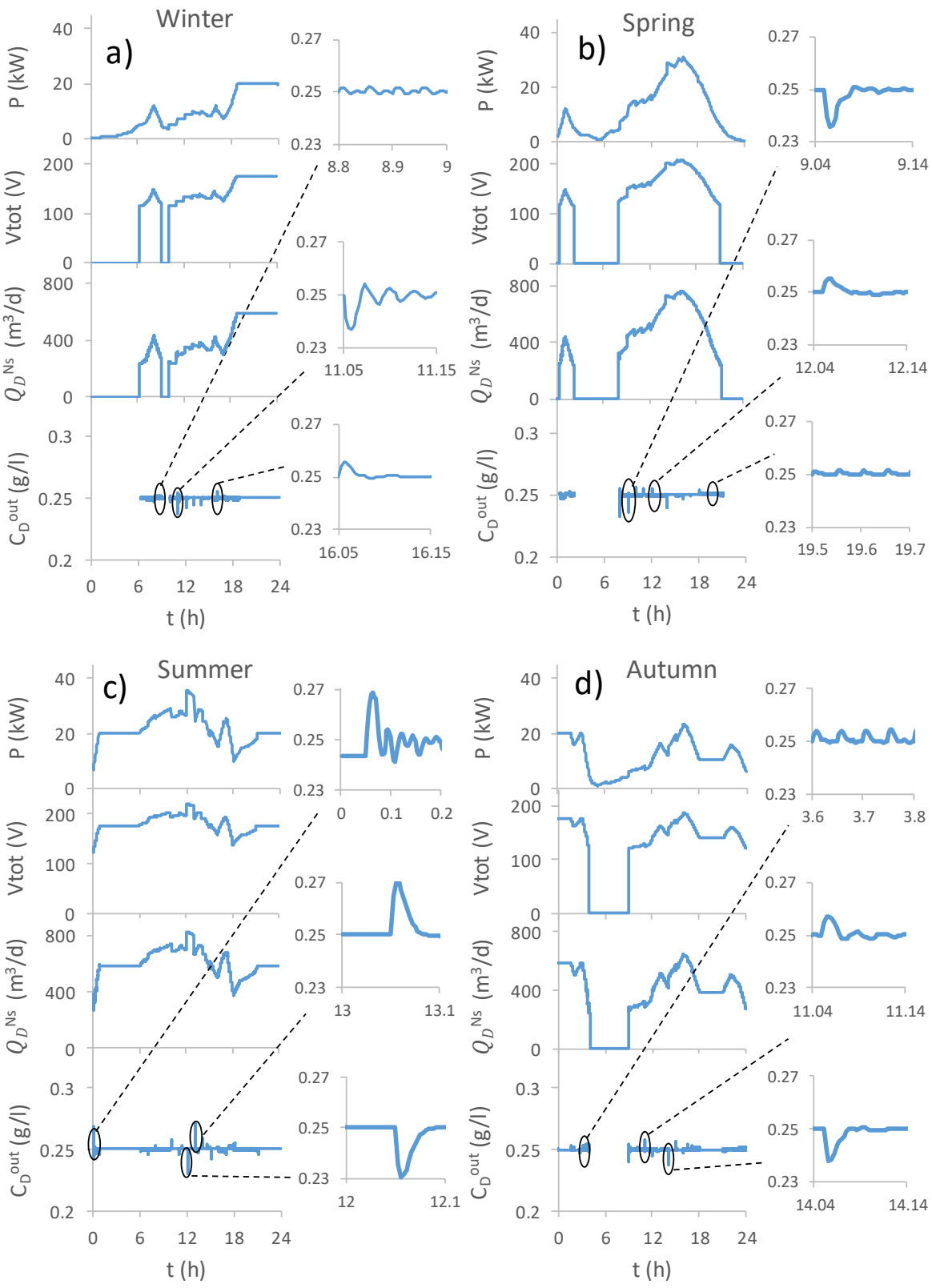

Figure 10. Results for daily simulations of the 4 ED stacks powered by a PV/Wind source equipped with a feedback controller. Graphs show available power, applied voltage, inlet flowrate and diluate outlet concentration (overall and dynamic details) for 4 days representative of a) Winter, b) Spring, c) Summer, d) Autumn. Units' specifications: 50x50 cm^2, 500 cell pairs, 270 μm spacers and FUJIFILM Type 10 membranes.

Simulation results for the daily operations are shown in Figure 10. For each day, the available power, the voltage applied to each ED unit, the plant diluate flowrate and the outlet diluate concentration are reported. During the sample winter day (Figure 10 a), power production is very low in the very first hours (i.e. before the sunset and with almost no wind). Then, some small power peaks are observed during light hours while the power grows up to 20 kW (i.e. the maximum capacity of the wind turbine) during the night due to an increased wind speed. This means that for the first hours of the days the unit is not able to operate as the power is below the power limit, while it keeps running for the rest of the day, except for an additional short period, reaching its maximum daily production in the last quarter of the day.

On the other hand, spring and autumn days (Figure 10 b and d) present a more unstable behaviour, characterised by a similar non-operational period of about 6 hours in between the first 2 quarters of the day and a power peak in the third quarter. The main differences between the two days is that the spring day shows a higher peak power production and higher peaks in the controlled concentration.

The summer reference day (Figure 10 c) is the only one in which plant operation is never interrupted, as the power produced by the PV/Wind hybrid system is always above the minimum threshold. Despite this, the day is characterised by a high number of steep variations, especially during light hours when solar irradiation keeps changing according to weather conditions. For this reason, the highest concentration peaks are observed during this day.

In addition to the overall daily data, some dynamic details of the control system action are also shown in Figure 10. For each day, a response to a positive and a negative step disturbance as well as to a ramp are highlighted. Relatively small peaks and fast responses are found for step disturbances (as discussed in the controller tuning section). Even in the summer day, characterised by the highest peaks, the outlet concentration stays below ± 10% of the set point value. In the same way, the oscillatory responses to ramp changes shows very limited oscillations around the set point.

6. CONCLUSIONS

The aim of this work has been to study the simulated behaviour of the single pass ED process when powered by a hybrid PV/Wind energy source. Simulations were performed through an ED process model in both a yearly and daily time scale.

In the yearly time scale, a quasi-steady state approach was adopted. 4 ED units working in parallel were simulated, in order to demonstrate how the process can work over the year within a wide range of flowrates (from a total diluate flowrate of 230 to 920m^3/d, corresponding to an absorbed power of 5 kW and 43 kW respectively, with this latter being 25% above the nominal operating condition), using the power produced by the variable power source. The plant is able to operate for most of the year, even though it switches off for short periods (especially during the winter) due to the excessively low power, reaching a cumulative operational period of more than 5500 hours.

On the other hand, daily simulations aimed to study detailed process dynamics. A control system based on Feedback and Feedforward controllers has been designed in order to to maintain the desired product concentration when the available power changes by acting on the feed flowrate. Simulating the power variation over different reference days, it was shown that

the controlled system works well in the entire range of flowrates, ensuring a stable operation and relatively short settling times of the outlet concentration, with maximum fluctuations lower than ± 10% of the set point. The advantages of adding a Feedforward controller to the traditional PID feedback controller resulted to be small and not so relevant for the operation in real operating scenarios.
Results indicated that, given the high flexibility and the fast and controllable process dynamics, ED proved its suitability for coupling with highly non-constant power sources. Therefore, the process could be successfully implemented in battery-less polygeneration systems for fresh water production, also acting as an energy buffer device.

ACKNOWLEDGMENTS

This work has been performed within the REvivED water project (Low energy solutions for drinking water production by a REvival of ElectroDialysis systems). The REvivED water project has received funding from the European Union's Horizon 2020 research and innovation programme under Grant Agreement no. 685579 (www.revivedwater.eu).

NOMENCLATURE

Symbols

A	Membrane area (m^2)
a	Axial induction factor
A_r	Rotor area (m^2)
B	Constant of WT model (K/km)
b	Membrane width (m)
C	Concentration (mol/m^3)
c_p	Wind turbine power coefficient
G_T	Insolation (W/m^2)
I	Current (A)
I_L	Photocurrent (A)
I_o	Diode reverse saturation current (A)
i	Current density (A/m^2)
J_{tot}	Total molar salt flux (mol/m^2s)
K	Process gain (g s/m^3 l)
k	Boltzmann constant (J/K)
K_C	Controller gain (m^3 l/g s)
L	Stack length (m)
N_{cp}	Number of cell pairs
N_M	Number of PV module connected in series

N_S	Number of ED stacks
p	Pressure (Pa)
Q	Volumetric flow rate (m^3/s)
q	Electron charge
q_w	Total water volumetric flux (m^3/m^2s)
R	Universal gas constant
R_{blank}	Blank specific electrical resistance (Ωm^2)
R_s	PV module series resistance (Ω)
R_{tot}	Cell pair specific electrical resistance (Ωm^2)
s	Independent variable in the Laplace domain
T	Temperature (K)
t	Time (s)
V	Voltage (V)
V_{cp}	Voltage drop over one cell pair (V)
V_{tot}	Overall voltage drop (V)
x	Coordinate in the direction of the main flow
z	Altitude (km)
α_w	Parameter of Von Karman correlation
γ	Empirical PV curve-fitting parameter
δ	Channel thickness (m)
ε	Error (g/l)
ε_G	Material bang gap energy
ζ	Damping coefficient
η	Non-Ohmic voltage drop (V)
$\mu_{I_{sc}}$	Temperature coefficient of I_{sc} at ref. condition (A/K)
$\mu_{V_{oc}}$	Temperature coefficient of V_{oc} at ref. condition (V/K)
ν	Wind speed (m/s)
ρ	Air density (kg/m^3)
τ_D	Derivative control time constant (s)
τ_I	Integral control time constant (s)

Abbreviations

AEM	Anion-exchange membrane

CEM	Cation-exchange membrane
ED	Electrodialysis
IMC	Internal model control
PV	Photovoltaic
RO	Reverse osmosis

Subscripts and superscripts

D	Dilute
$elev$	Height above the ground (elevation)
in	Inlet
mp	Point of maximum power
N_s	Number of stacks
oc	Open-circuit
ref	Reference condition
sc	Short-circuit
SOL	Solution (either concentrate or diluate)
ss	Steady state
tot	Total

REFERENCES

1. Cardona E, Culotta S, Mangiaracina L, Terranova R. Multi-flash desalination and cogeneration to solve the water supply problems in southeastern Sicily. Desalination 1996;106:121–30. doi:10.1016/S0011-9164(96)00100-2.
2. Kamal I. Cogeneration desalination with reverse osmosis: A means of augmenting water supplies in Southern California. Desalination 1992;88:355–69. doi:10.1016/0011-9164(92)80127-U.
3. Khan EU, Martin AR. Optimization of hybrid renewable energy polygeneration system with membrane distillation for rural households in Bangladesh. Energy 2015;93:1116–27. doi:10.1016/J.ENERGY.2015.09.109.
4. Usón S, Uche J, Martínez A, del Amo A, Acevedo L, Bayod Á. Exergy assessment and exergy cost analysis of a renewable-based and hybrid trigeneration scheme for domestic water and energy supply. Energy 2019;168:662–83. doi:10.1016/J.ENERGY.2018.11.124.
5. Calise F, de Notaristefani di Vastogirardi G, Dentice d'Accadia M, Vicidomini M. Simulation of polygeneration systems. Energy 2018;163:290–337. doi:10.1016/J.ENERGY.2018.08.052.
6. Jana K, Ray A, Majoumerd MM, Assadi M, De S. Polygeneration as a future sustainable energy solution – A comprehensive review. Appl Energy 2017;202:88–111. doi:10.1016/J.APENERGY.2017.05.129.
7. Calise F, Dentice d'Accadia M, Vanoli R, Vicidomini M. Transient analysis of solar polygeneration systems including seawater desalination: A comparison between linear Fresnel and evacuated solar collectors. Energy 2019;172:647–60. doi:10.1016/J.ENERGY.2019.02.001.
8. Sahoo U, Kumar R, Pant PC, Chaudhary R. Development of an innovative polygeneration process in hybrid solar-biomass system for combined power, cooling and desalination. Appl Therm Eng 2017;120:560–7. doi:10.1016/J.APPLTHERMALENG.2017.04.034.
9. Esrafilian M, Ahmadi R. Energy, environmental and economic assessment of a polygeneration system of local desalination and CCHP. Desalination 2019;454:20–37. doi:10.1016/J.DESAL.2018.12.004.
10. Calise F, Macaluso A, Piacentino A, Vanoli L. A novel hybrid polygeneration system supplying energy and desalinated water by renewable sources in Pantelleria Island. Energy 2017;137:1086–106. doi:10.1016/J.ENERGY.2017.03.165.
11. Calise F, Dentice d'Accadia M, Macaluso A, Vanoli L. A novel solar-geothermal trigeneration system integrating water desalination: Design, dynamic simulation and economic assessment. Energy 2016;115:1533–47. doi:10.1016/J.ENERGY.2016.07.103.
12. Calise F, Dentice d'Accadia M, Piacentino A. Exergetic and exergoeconomic analysis of a renewable polygeneration system and viability study for small isolated communities. Energy 2015;92:290–307. doi:10.1016/J.ENERGY.2015.03.056.
13. Calise F, Cipollina A, Dentice d'Accadia M, Piacentino A. A novel renewable polygeneration system for a small Mediterranean volcanic island for the combined production of energy and water: Dynamic simulation and economic assessment. Appl Energy 2014;135:675–93. doi:10.1016/J.APENERGY.2014.03.064.
14. Manolakos D, Mohamed ES, Karagiannis I, Papadakis G. Technical and economic comparison between PV-RO system and RO-Solar Rankine system. Case study: Thirasia island. Desalination 2008;221:37–46. doi:10.1016/J.DESAL.2007.01.066.
15. Karimi L, Abkar L, Aghajani M, Ghassemi A. Technical feasibility comparison of off-

grid PV-EDR and PV-RO desalination systems via their energy consumption. Sep Purif Technol 2015;151:82–94. doi:10.1016/j.seppur.2015.07.023.
16. Garg MC, Joshi H. A Review on PV-RO Process: Solution to Drinking Water Scarcity due to High Salinity in Non-Electrified Rural Areas. Sep Sci Technol 2015;50:1270–83. doi:10.1080/01496395.2014.951725.
17. Shawky HA, Abdel Fatah AA, Abo ElFadl MMS, El-Aassar AHM. Design of a small mobile PV-driven RO water desalination plant to be deployed at the northwest coast of Egypt. Desalin Water Treat 2015;55:3755–66. doi:10.1080/19443994.2015.1080447.
18. Helal AM, Al Malek SA, Al Hammadi EM, Al-Thani HA. Economic feasibility of grid-connected PV-RO and PV-MVC small desalination units for remote areas in The United Arab Emirates — A comparative study. Desalin Water Treat 2009;3:241–51. doi:10.5004/dwt.2009.466.
19. El-Shaarawi MAI, Al Awjan H, Al Ramadhan D, Hussain M. Effect of thermodynamic limitations on PV initial cost estimations for solar-powered RO desalination. Desalination 2011;276:28–37. doi:10.1016/J.DESAL.2011.03.021.
20. Clarke DP, Al-Abdeli YM, Kothapalli G. The effects of including intricacies in the modelling of a small-scale solar-PV reverse osmosis desalination system. Desalination 2013;311:127–36. doi:10.1016/J.DESAL.2012.11.006.
21. Thomson M, Infield D. A photovoltaic-powered seawater reverse-osmosis system without batteries. Desalination 2003;153:1–8. doi:10.1016/S0011-9164(03)80004-8.
22. Thomson M, Infield D. Laboratory demonstration of a photovoltaic-powered seawater reverse-osmosis system without batteries. Desalination 2005;183:105–11. doi:10.1016/J.DESAL.2005.03.031.
23. Carta JA, González J, Subiela V. The SDAWES project: An ambitious R and D prototype for wind-powered desalination. Desalination 2004;161:33–48. doi:10.1016/S0011-9164(04)90038-0.
24. García-Rodríguez L. Desalination by Wind Power. Wind Eng 2005;28:453–63. doi:10.1260/0309524042886405.
25. Caldera U, Bogdanov D, Breyer C. Local cost of seawater RO desalination based on solar PV and wind energy: A global estimate. Desalination 2016;385:207–16. doi:10.1016/J.DESAL.2016.02.004.
26. Lundstrom JE. Water desalting by solar powered electrodialysis. Desalination 1979;31:469–88. doi:10.1016/S0011-9164(00)88551-3.
27. Ishimaru N. Solar photovoltaic desalination of brackish water in remote areas by electrodialysis. Desalination 1994;98:485–93. doi:10.1016/0011-9164(94)00175-8.
28. Malek P, Ortiz JM, Schulte-Herbrüggen HMA. Decentralized desalination of brackish water using an electrodialysis system directly powered by wind energy. Desalination 2016;377:54–64. doi:10.1016/j.desal.2015.08.023.
29. Ortiz JM, Expósito E, Gallud F, García-García V, Montiel V, Aldaz A. Photovoltaic electrodialysis system for brackish water desalination: Modeling of global process. J Memb Sci 2006;274:138–49. doi:10.1016/j.memsci.2005.08.006.
30. Ortiz JM, Expósito E, Gallud F, García-García V, Montiel V, Aldaz A. Electrodialysis of brackish water powered by photovoltaic energy without batteries: direct connection behaviour. Desalination 2007;208:89–100. doi:10.1016/J.DESAL.2006.05.026.
31. Ortiz JM, Expósito E, Gallud F, García-García V, Montiel V, Aldaz VA. Desalination of underground brackish waters using an electrodialysis system powered directly by photovoltaic energy. Sol Energy Mater Sol Cells 2008;92:1677–88. doi:10.1016/j.solmat.2008.07.020.
32. Campione A, Cipollina A, Bogle IDL, Gurreri L, Tamburini A, Tedesco M, et al. A hierarchical model for novel schemes of electrodialysis desalination. Desalination

2019;465:79–93. doi:10.1016/j.desal.2019.04.020.
33. Klein Sa, Beckman WA, Mitchell JW, Duffie JA, Duffie NA, Freeman TL. Solar energy laboratory, TRNSYS. A Transient Syst Simul Program Univ Wisconsin, Madison 2006.
34. Koeppl, G.W. Putnam's power from the wind. Van Nostrand Reinhold Company,New York, NY; 1982.
35. Gurreri L, Tamburini A, Cipollina A, Micale G, Ciofalo M. CFD prediction of concentration polarization phenomena in spacer-filled channels for reverse electrodialysis. J Memb Sci 2014;468:133–48. doi:10.1016/j.memsci.2014.05.058.
36. Gurreri L, Tamburini A, Cipollina A, Micale G, Ciofalo M. Flow and mass transfer in spacer-filled channels for reverse electrodialysis: a CFD parametrical study. J Memb Sci 2016;497:300–17. doi:10.1016/j.memsci.2015.09.006.
37. Gurreri L, Ciofalo M, Cipollina A, Tamburini A, Van Baak W, Micale G. CFD modelling of profiled-membrane channels for reverse electrodialysis. Desalin Water Treat 2015;55:1–20. doi:10.1080/19443994.2014.940651.
38. La Cerva M, Gurreri L, Tedesco M, Cipollina A, Ciofalo M, Tamburini A, et al. Determination of limiting current density and current efficiency in electrodialysis units. Desalination 2018;445:138–48. doi:10.1016/J.DESAL.2018.07.028.
39. Seborg DE, Edgar TF, Mellichamp DA, Doyle FJ. Process dynamics and control. Wiley; 2016.